Aerodynamic Characterization of the IEA 15 MW Reference Wind Turbine by Code-to-Code Comparison

Journal of Physics: Conference Series **2767** (2024) 022040 doi:10.1088/1742-6596/2767/2/022040

Aerodynamic Characterization of the IEA 15 MW Reference Wind Turbine by Code-to-Code Comparison

Lorenzo Tieghi[1], Vincenzo Morici[1], Alessio Castorrini[1], Navid Aryan[1] and Luca Greco[2]

[1] Department of Mechanical and Aerospace engineering (DIMA), Sapienza University of Rome, Via Eudossiana 18, 00184, Rome, Italy.
[2] CNR-INM - Institute of Marine Engineering, Via di Vallerano 139, 00128 Rome, Italy.

E-mail: luca.greco@cnr.it

Abstract. The consistency of different aerodynamic formulations applied to the analysis of a modern multi-megawatt horizontal axis wind turbine rotor is investigated. The proposed code-to-code comparison involves specific implementations of a hierarchy of solvers based on Blade Element Momentum Theory (*AEOLIAN*), Actuator Line Modelling (*OpenFOAM*), free-wake Panel Method (*FUNAERO*) and blade-resolved Computational Fluid Dynamics (*OpenFOAM*). The analysis addresses local and integral aeroloads and flow physical quantities concerning the state-of-the-art IEA 15 MW reference wind turbine in axial uniform flow conditions. The proposed solvers predict consistent rotor performance and blade aeroloads (also in line with data from of IEA Task 47). However, differences emerge close to blade root, where blade-resolved CFD reveals a significant flow separation on the suction side. Furthermore, scattering of induction factors computations is observed, especially in the axial direction. Different methodologies and numerical setup used in blade-resolved simulations allow achieving physically-consistent induction values, especially at blade tip. Finally, flow-field predictions by Computational Fluid Dynamics (CFD) and Panel Method are consistent upstream and close to the disk downstream (except where significant flow separation occurs), whilst a more detailed study on the effect of extending wake refinement zone in CFD simulation is advisable.

1. Introduction

The constant effort towards new generation of multi-megawatt wind turbines (WTs) with longer and more flexible blades has captured the interest of the scientific community. In this context, collaborative research outcomes of the IEA Wind Tasks [1, 2] demonstrate that WT aerodynamics modelling remains challenging, especially in off-design conditions. This scenario is even more complex for floating WTs, where this challenge must be faced within a multidisciplinary context involving rotary-wing aerodynamics, tower and blades structural dynamics, floater/waves interaction and control strategies.

The availability of well-assessed aerodynamic formulations is hence fundamental. The low-fidelity engineering models based on Blade Element Momentum Theory (BEMT) [3], although being widely used by the industry for aeroservoelastic applications, gradually show limitations when rotors with complex blades shape working in highly unsteady conditions are considered [1]. At a higher fidelity level, hybrid models, such as the Actuator Line Model (ALM) [4] and Free-Vortex Wake models [5] have shown to be very reliable in different operating

conditions, although their accuracy critically depends on the appropriateness of input airfoil lift and drag characteristics [1]. On the other side, Computational Fluid Dynamics (CFD) [1, 6] yields physically consistent predictions of turbine aerodynamics although at considerable computational costs. Hence, its application is challenging for aeroelastic simulations, particularly in the early design stages. This limitation becomes more apparent when considering the extensive aeroservoelastic analyses required by the IEC-61400 regulations. Finally, a good trade-off among accuracy, CPU time demand and out-of-the-box functionality is represented by potential flow Panel Methods which have demonstrated close alignment with experimental results in different operating conditions [7,8]. The main limitation of this type of solvers lies in the rough modelling (if any) of viscosity-driven effects (see *e.g.*, [8] and [5]) requiring suitable modelling [9].

The continuous assessment and improvement of these numerical tools is a critical aspect requiring a holistic approach, considering both global and local physical quantities. Several code-to-code comparisons have revealed inherent limitations in the capabilities of all aerodynamic formulations [1] and ambiguities may arise in determining their proper implementation and application. Hence, a complementary approach comparing numerical models of both different and same accuracy level is the optimal choice for the comprehension of WT aerodynamics and the assessment of tools with broader applicability ranges [1]. The present work contributes to this aim by comprehensively investigating the capabilities and limitations of specific implementations of four solvers based on BEMT, ALM, free-wake Panel Method and CFD applied to the aerodynamic analysis of the state-of-art IEA 15 MW reference WT [10] which is focal point for the simulation activities performed within the IEA Task 47.

The paper is organized as follows: Section 2 outlines an overview of the proposed solvers, numerical results are discussed in Section 3, and the main conclusions are reported in Section 4.

2. Rotor aerodynamics modelling: methodologies and numerical setup

2.1. Blade-Resolved CFD

The incompressible blade-resolved CFD (BR-CFD) simulation of the turbulent viscous flow field relies on the solution of the pressure-based steady Reynolds Averaged Navier–Stokes (RANS) equations. Turbulence model has been selected following a preliminary comparison between four closure models: $k-\varepsilon$, $k-\omega$, cubic $k-\varepsilon$ and the two-equation Menter's $k-\omega$ shear stress transport (SST) [11], with $k-\omega$ SST computations exhibiting greater consistency with the results of the other codes. The system of equations is solved using the SIMPLE-C algorithm of OpenFOAM-v. 2306 [12]. An under-relaxation factor equal to 0.3 is applied to the pressure field, whilst a factor of 0.5 is applied to the momentum and turbulence quantities. The space discretization of all conservation laws uses a second order upwind scheme. The simulation is carried out on a single periodic rotor sector of 120° including one of the three blades, in a domain extending 10 diameters upstream, downstream and radially. The computational domain entails 51M cells and is discretized using a hybrid mesh, with 33M hexahedral elements near the blade walls, to form an inflation layer with a growth rate of 1.1 extending up to 2 cords normal to the blade surface. Tetrahedral elements are used to discretize the rest of the domain, with 15M cells located within 1 diameter from the blade surface. The grid is designed for high-Reynolds computations, with first cell center placed at 0.3 mm from the solid surfaces and maximum a-posteriori y^+ value of 110 at the blade tip. This mesh setup has been selected as a result of a sensitivity analysis which is omitted for brevity. The equations are solved in the rotating frame of reference rigidly connected to the rotor and centered at the shaft. The number of SIMPLE-C iterations is set to 20000 to assure the convergence of the flow field and forces.

At the domain inlet, constant conditions are imposed to all quantities, with an inflow velocity U_∞, turbulence intensity $TI = 6\%$ and assuming the rotor radius as the turbulent reference length scale. Periodic cyclic conditions are imposed on the domain's side boundaries, while the spinnercone and the nacelle are simplified through a no-friction cylindrical surface having the

hub radius. Standard high-Reynolds wall functions are applied for the blade wall boundary conditions.

2.2. Panel Method

FUNAERO (*Free-wake UNsteady AERODynamics*) is a 3D unsteady aerodynamic solver well-assessed over a wide range of operating conditions for wind turbine applications [1, 7, 8, 13]. It is based on the solution of the Laplace equation ($\nabla^2\varphi = 0$) governing the perturbation velocity field around 3D lifting bodies in arbitrary motion under the assumption of inviscid and irrotational flows. This is achieved by the unbounded-space Green function technique [14], providing a Boundary Integral Equation (BIE) for the velocity potential on the turbine surface, accounting for the presence of the bodies via a superposition of singularities distributed on the actual surface of rotor blades $\mathcal{S}_B$ and their wakes $\mathcal{S}_W$; the impermeability condition on the blades and the absence of pressure discontinuity and fluid particles motion throughout the wake define the corresponding boundary conditions [15].

Numerically, a *zero-th* order Boundary Element Method (BEM) is used to solve the problem for φ by discretization of $\mathcal{S}_B$ and $\mathcal{S}_W$ into surface panels and enforcing the BIE at their centroids on $\mathcal{S}_B$. Finally, blade pressure is computed by the Bernoulli equation and aerodynamic loads are obtained through surface integration of the surface pressure field and stresses associated with viscosity. Viscous terms are here (roughly) estimated by assuming that the boundary layer of each blade section behaves like that over an *equivalent flat plate* at the same Reynolds number.

A robust free-wake solution procedure is adopted to determine rotor wake shape by aligning wake points to the local velocity field due to both the incoming wind and the rotor/wake ($\nabla\varphi$). The latter comes from the computation of $\nabla\varphi$ on $\mathcal{S}_W$ with wake self-induced contribution computed using the Biot-Savart law coupled with the vortex-core model proposed in [15]. Numerically, starting from a suitable initial guess for $\mathcal{S}_W$, a predictor/corrector-type finite difference method based on the Heun scheme [16] is adopted to solve wake points transport equation [8]. This procedure is iterated up to a steady (periodic) solution is achieved.

Numerical predictions by *FUNAERO* rely on discretization settings coming from a preliminary convergence analysis (not shown here) ensuring negligible sensitivity of rotor loads to further refinement. For a single blade, the number of panels in chordwise and spanwise direction (M_B and N_B) are equal to 38 and 60, respectively. The overall wake revolutions are $W_R = 10$ each consisting of $N_W = 60$ panels, streamwise. For the present computations, the nacelle and tower are not considered. The steady free-wake analysis is governed by a pseudo-time step $\Delta t = 1/nN_W$ (being n the rotor rotation per second). Finally, the nondimensional vortex core radius ($r_c = 0.01D$) and growth factor ($\epsilon = 5$) are chosen accordingly to the incoming wind velocity [8].

2.3. Actuator Line Model

The Actuator Line Model (ALM), proposed in [4], simulates the effect of the rotor on the flow-field by replacing the 3D blade geometry with a superposition of momentum sources in the Navier-Stokes equations. Present computations are based on *turbinesFoam* [17], an open-source implementation of the ALM in OpenFOAM. The library has been properly modified to include blade elasticity and multiple-reference body motion capabilities to allow the aeroelastic simulation of floating offshore WTs [18]. Numerically, the blades are modelled as a series of localized momentum sources with a magnitude depending on the local geometry and flow properties. Similarly to BEMT-based approaches, section aerodynamic forces are computed by a look-up table process based on lift and drag input data.

In the current application, the actuator line is the geometric locus of the aerodynamic centers of the sections and is discretized into a series of 98 equally-spaced elements. A tip/root loss correction based on the lifting line theory is applied to the lift coefficient [19]. Turbulence modelling relies on the $k-\omega$ SST model. The numerical domain extends 15D and 10D

in streamwise and cross-flow directions, with the rotor located at 5D from the inlet. This domain setup has been selected after a sensitivity analysis not shown here for conciseness. The computational grid entails 1.1M hexahedral isotropic cells and includes three refinement regions, based on the distance from the rotor, to properly capture near and far wake, with the smallest characterized by a 2.5 m length and thus maintaining the element-cell length ratio below the maximum of 0.75 identified in [20]. Inflow and outflow boundary conditions are consistent with the BR-CFD setup. Computations are based on the PISO algorithm with backward implicit time integration scheme and a fixed time step of 0.025 s. This setup ensures that the tip element spans less than one cell each iteration.

2.4. Blade Element Momentum Theory

AEOLIAN (*AErOeLastic sImulAtioN*) is an engineering-type solver based on the two-way strong coupling between an in-house implementation of BEMT and a Lumped-Mass model for blade structure. It is developed within MATLAB Simulink/Simscape-Multibody© environment and has been previously validated against different comprehensive aeroelastic tools [21].

The aerodynamic solver of *AEOLIAN* herein used, discretize the blade using 50 sections and is based on the non-iterative methodology introduced in [22] which parameterize BEMT equations [23, 24] with respect to one variable (*i.e.*, the local inflow angle, ϕ) reducing the set of two nonlinear equations for the axial (a) and tangential factor (a') to one. The corresponding residual form for ϕ is then solved using the robust one-dimensional Brent's method [25]. Unlike typical implementations, which use iterative solution methods to converge the induction factors (e.g., fixed-point iteration or Newton's method), this approach was originally built for gradient-based optimization and proved to be convergent in every instance [22].
In addition to the proposed BEMT model, *AEOLIAN* uses Prandtl tip/hub loss [3] correction to take the discrete number of blades into account and Glauert/Buhl [26] to empirically model high-induction conditions.

3. Numerical results

Aerodynamics computation of the IEA 15 MW rotor in uniform axial flow is herein addressed at $U_\infty = 7.5\ m/s$ and 5.33 RPM (below-rated). This turbine features an upwind rotor with a diameter $D = 240.8$ m and three blades, each preconed (4°) and prebent. In addition to the solvers described in Section 2, blade-resolved CFD computations from Fraunhofer Institute for Wind Energy Systems (IWES) obtained with *OpenFOAM-v4* and BEMT data from *Aerodyn-v15* are included in the code-to-code comparison. The input rotor geometry and airfoils lift and drag curves (for BEMT- and ALM-based codes) are the same for all models and are consistent with the definition reported in [10]. In details, airfoil characteristics are corrected for rotational stall delay effects by using the Selig and Eggars method and then extrapolated up to ±180° through the Viterna correction. Differently, no correction is applied to the pitching moment [10].

3.1. Rotor and blade loads

The analysis of rotor performance, summarized in Table 1, shows how present thrust predictions exhibit a reduced scattering with respect to available CFD and BEMT data. Notably, *FUNAERO* and BR-CFD (*OpenFOAM-v23*) predict the same amount of torque, whilst the resolved CFD shows a 3.3% higher thrust. Among the different codes, the highest torque comes from ALM-based computations (1.8% with respect to present BR-CFD), with a mild underprediction of thrust as against other methods. A comparison between *AEOLIAN* and the medium-fidelity models highlights that the former exhibits the lowest torque (−3.7% with respect to *FUNAERO*), while thrust is close to the observed average prediction. As a final remark, the medians of torque and thrust predicted by the proposed solvers are 1.08×10^7 Nm and 1.22×10^6 N, respectively. Correspondingly, the maximum variance of the present predictions is about 3% for both torque and thrust.

Table 1: Code-to-code comparison of rotor performance.

Simulation	Code	Torque [Nm]$\times 10^7$	Thrust [N]$\times 10^6$
Literature, BR-CFD	*OpenFOAM-v4*	0.99	1.17
Literature, BEMT	*Aerodyn-v15*	1.00	1.27
Present, BR-CFD	*OpenFOAM-v23*	1.08	1.25
Present, Panel Method	*FUNAERO*	1.08	1.21
Present, ALM	*OpenFOAM-v22*	1.10	1.20
Present, BEMT	*AEOLIAN*	1.04	1.23

The analysis of blade section normal (F_{n_c}) and tangent-to-the-chord (F_{t_c}) forces in Fig.1 provides a quantitative indication of the source of the observed deviations among the different codes. As a general comment, all models show consistent predictions of F_{n_c} at mid-span sections (48 m $< r <$ 84 m) although present BR-CFD indicates higher loading levels with a maximum deviation of about 3.5% with respect to *FUNAERO* and IWES BR-CFD computations. At the same sections, slightly larger scattering of results is observed for F_{t_c} where *FUNAERO*, *AEOLIAN* and ALM consistently predict lower loading with respect to the higher-fidelity model (with an average of $5-8\%$ deviation) and about $5-6\%$ higher than IWES BR-CFD. Higher loading with respect to IWES BR-CFD data (about 5%) is predicted at the peak F_{n_c} by BR-CFD and *AEOLIAN*, whereas the outcome of *FUNAERO* is in line with IWES data. In this blade portion, the ALM shows an anticipation of maximum F_{n_c} location. Similar conclusions come from the assessment of F_{t_c}, except for the higher consistency of *AEOLIAN* results with respect to IWES BR-CFD data.

Viscosity-driven flow effects become gradually significant towards the blade root. Indeed, present BR-CFD predicts the onset of flow separation at the suction side between $r = 14$ m and $r = 40$ m (see Fig.2 showing the velocity streamlines on blade surface) leading to an increase of viscosity-induced torque losses. The corresponding load reduction is captured only by the higher-fidelity BR-CFD solvers and, slightly, by the ALM and BEMT-based approaches. Differently, the rough modelling of viscous stresses in *FUNAERO* contributes to the overestimation of F_{n_c} and F_{t_c} in this blade portion. Finally, towards blade tip, all solvers tend to provide consistent predictions, with the ALM showing lower normal loading due to the anticipation of the peak F_{n_c}. Similar observations can be drawn from the analysis of blade section normal (F_{n_r}) and tangent-to-the-rotor disk (F_{t_r}) forces (not shown here for conciseness).

3.2. Blade pressure distribution

Blade pressure distribution is investigated by the blade-resolved codes. Figure 3 shows the chordwise distribution of the pressure coefficient $C_p = (p - p_\infty)/\rho(nD)^2$ (herein p_∞ is the unperturbed pressure and $\rho = 1.225$ kg/m^3 the air density) along three radial stations, namely $r/R = 0.24$, 0.64 and 0.85. As expected, the panel code exhibits an excellent prediction of C_p on the pressure side (PS) from $r/R = 0.44$ going outboard, with differences on the suction side (SS) gradually increasing inboard. Additionally, it is observed that grid refinement is necessary for the panel code at the blade leading edge to accurately capture local pressure peaks. As a general comment, consistently with blade loads analysis (where *FUNAERO* predicts lower loads than CFD), the pressure difference between SS and PS is lower than present BR-CFD results at all radial stations except close to the root where BR-CFD data clearly indicates a wide region of separated flow starting at $x/c = 0.5$.

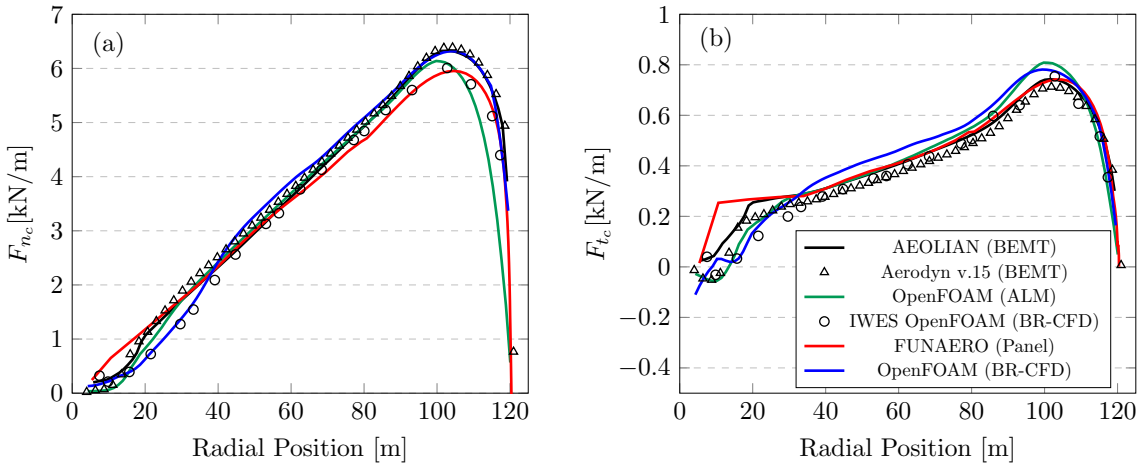

Figure 1: Spanwise distribution of (a) normal- and (b) tangential-to-chord aerodynamic forces.

Figure 2: Blade pressure and suction side velocity streamlines - OpenFOAM (BR-CFD).

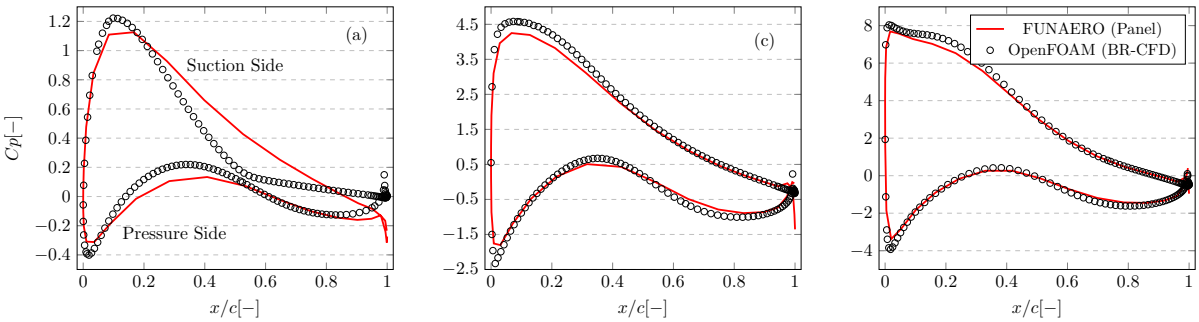

Figure 3: Predicted blade pressure coefficient at $r/R = 0.24$, 0.64 and 0.85 (a-c). $x/c = 0$ and $x/c = 1$ correspond to the leading and trailing edge, respectively.

3.3. Induction factors and angle of attack

A correct evaluation of the induction factors is critical for the accuracy of engineering models. The sketch in Fig.4, where xyz is a non-rotating frame of reference centered at the hub, shows the location of blade points where the axial ($a = v_a^i/V_\infty$) and tangential ($a' = v_t^i/\Omega R$) induction

factors are computed, being v_a^i and v_t^i rotor wake induced velocity along x and y, respectively.

The methodology for the computation of a and a' and the location of the corresponding Induction Computation Points (ICPs) is illustrated next. For the present analysis, AoA and induction factors are computed at the quarter-chord point of the reference blade section (red line in the left portion of Fig.4).

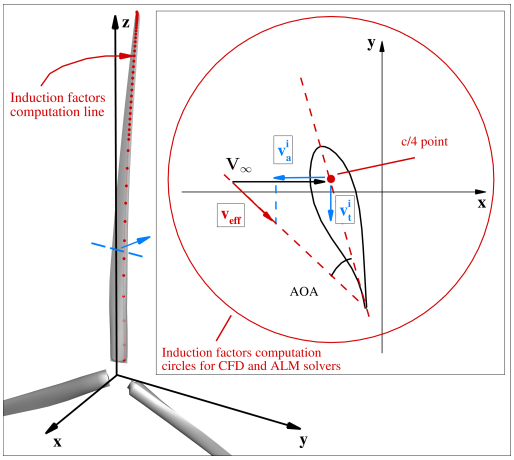

Figure 4: Location of induction factors computation points.

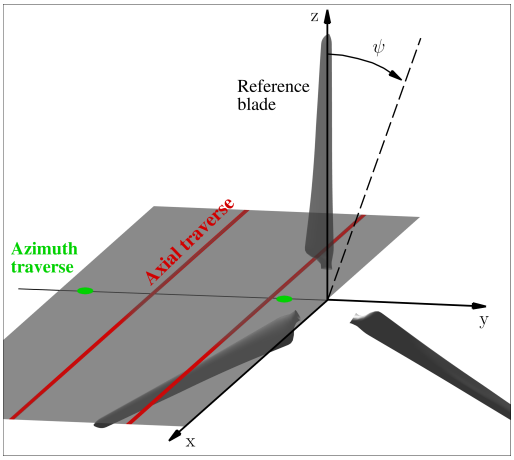

Figure 5: Layout of velocity field computation points.

Within the ALM and BR-CFD, two different methods to compute a and a' are considered: *i)* the Line Average Method (LAM) [27] where the velocities are averaged along a circle centered at $c/4$ with the radius equal to the sectional chord c (see Fig.4); *ii)* the Azimuthal Averaging Technique (AAT) proposed in [28] where, for each radial location, the azimuthal average of the velocity computed on upstream and downstream rings are used to interpolate the induction at the ICPs. Differently, in *FUNAERO*, the induced velocity field is computed by taking the gradient of the Boundary Integral Representation for velocity potential at the ICPs (see Section 2.2). It is worthy note that the AAT and LAM procedure are based on potential flow assumptions (just as the Panel Code) and they merely approximate the removal of the influence of reference blade circulation from the induced velocity field (see [27] for further details). Differently, in *FUNAERO*, reference blade circulation is neglected by numerically removing the singularities placed on its surface.

Figures 6a and 6b show the spanwise distribution of a and a', respectively, where ALM and BR-CFD predictions are based on the AAT. At blade mid-span (48 m $< r <$ 96 m), BR-CFD and Panel Method provide consistent axial induction predictions, whilst the lower fidelity models show higher levels. Elsewhere, a significant scattering of results is observed: the ALM and BR-CFD show similar results at the tip, whilst the lower axial perturbation velocity due to flow separation towards the root, is captured only by the BR-CFD solver. Overestimated values of a are also predicted by *FUNAERO* outboard starting from $r = 105$ m. The consistency of geometry-resolved predictions close to blade tip is further investigated in Fig. 7. In details, the inherent velocity averaging process of the AAT produces a smooth behaviour of a at the very tip. A similar result is obtained by numerically increasing the vortex core radius from $r_c^A = 0.01D$ (*i.e.*, the one used for the free-wake computations) to $r_c^B = 0.04D$ in *FUNAERO* computations (see Section 2.2) yielding an excessive filtering of the tip vortex effect. Differently, the Line Average Method provides more *local* velocity values exhibiting a close match with the outcomes of *FUNAERO* obtained with the core radius r_c^A. Similar considerations hold for a' (see Figure 6b, where ALM and BR-CFD predictions are based on the AAT). Although in this case *Aerodyn-v15*, *AEOLIAN* and *FUNAERO* outcomes perfectly match along the full span except

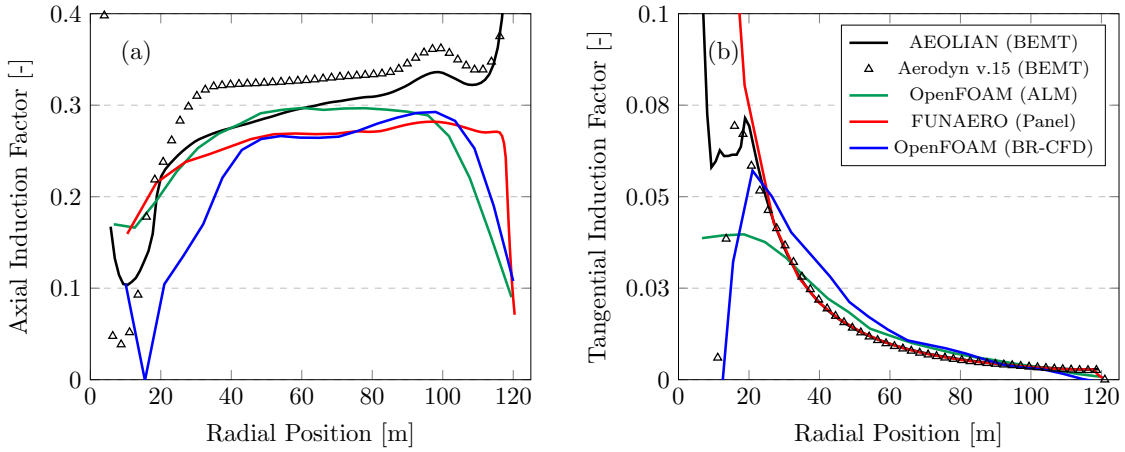

Figure 6: Spanwise distribution of axial (a) and tangential (b) induction factors.

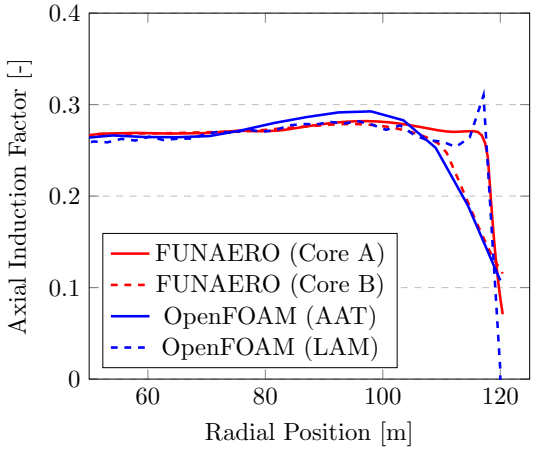

Figure 7: Analysis of the axial induction factor close to blade tip.

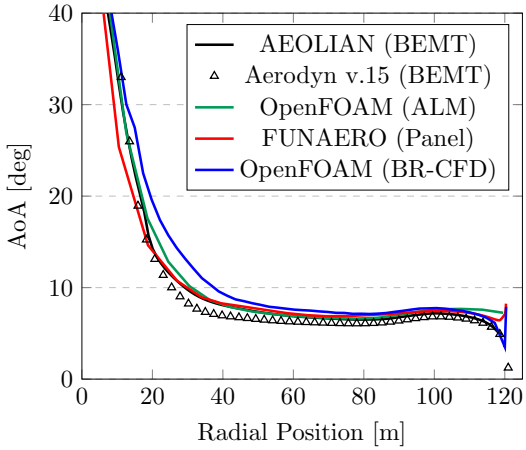

Figure 8: Spanwise distribution of angle of attack.

close to blade root, the ALM and BR-CFD predict higher levels of induction except inboard, where the effect of flow separation is evident especially in BR-CFD computations.

The spanwise distribution of AoA is depicted in Fig. 8. The computation of AoA in BR-CFD and ALM is based on the *Line Average Method,* whereas a vortex core radius $r_c^A = 0.01D$ is used in *FUNAERO*. Consistently with Figs. 6 and 7 all proposed solvers provide similar outcomes at mid-span (with *Aerodyn-v15* constantly showing lower AoAs). Differences arise both at blade root (due to the flow separation observed in Fig. 2) and tip where geometry-resolved codes predict an increase of AoA. Indeed, in this blade area, 3D effects become gradually relevant, hence blade sections cannot be considered equivalent to 2D airfoils working at suitably computed AoAs. Differently, Prandtl tip-loss correction [3], implemented in *Aerodyn-v15* and *AEOLIAN*, modifies a to achieve null loading at blade tip. Hence, as confirmed also by the analysis in [1], a decreasing *equivalent* AoA is predicted by BEMT-based codes.

3.4. Velocity field

The velocity field prediction past the rotor is herein addressed. The layout used for this analysis is shown in Fig.5. The selected locations for the (absolute) velocity computation in the xy plane are: i) two axial traverses (red lines) placed at $y/R = 0.2$ (inner, $y = 24$ m) and $y/R = 0.7$ m (outer, $y/R = 84$ m), respectively, where velocities are collected whenever the reference blade passes at 12 o'clock position ($\psi = 0°$) at points located from $x = -1D$ to $x = 1D$ (the rotor

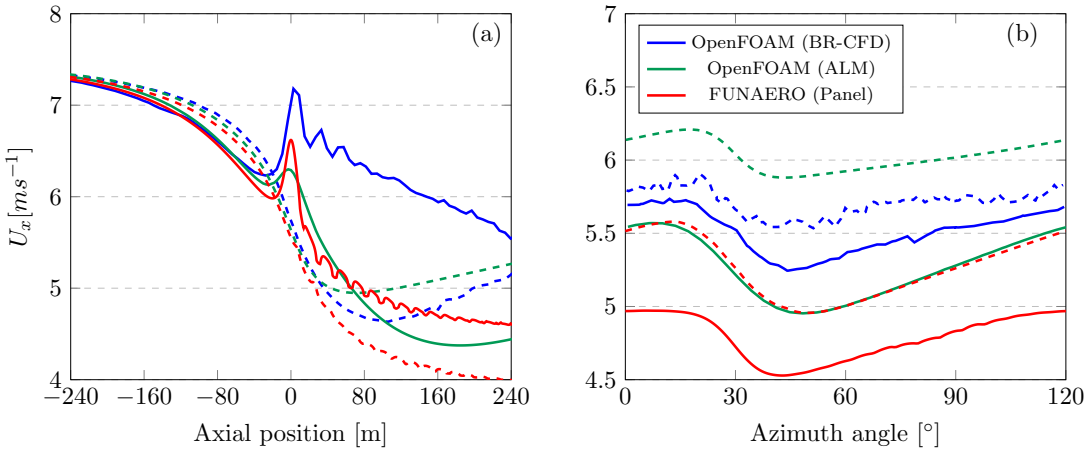

Figure 9: Axial (a) and azimuth (b) velocity traverse at inner (solid) and outer (dashed) radii.

is located at $x = 0$); *ii*) an azimuth traverse of 120° where the measuring points are located downstream at $x = 15.6$ m ($x/R = 0.13$) and $r/R = 0.35$ and 0.92 (green points). Axial (U_x) velocity is positive along x. Figure 9a shows U_x along the axial traverse, computed in the refined portion of the CFD mesh (up to 1D down- and upstream the rotor). At $x < 0$, CFD, ALM and Panel Method consistently predict the flow deceleration (with respect to the unperturbed condition) caused at both radii by the rotor blockage effect. Moving towards the rotor disk, a local flow acceleration just upstream the thick blade root passage is predicted by all solvers at the inner radius (although with different intensity). Downstream, good consistency is observed up to $x = 40$ m at the outer radius. As the distance from the disk increases, potential-flow computations anticipate lower velocity in comparison to both CFD and ALM (which exhibit parallel trends). At the inner radius, the effect of a very high AoA (corresponding to the low axial induction) leads to a larger magnitude of U_x. This occurrence is predicted by CFD, whilst ALM and *FUNAERO* show significantly lower velocity values (although with similar trend).

Finally, considering the azimuth traverse (Fig.9b), blade-resolved codes and the ALM (although with slightly different magnitude) capture the axial velocity perturbation due to the intersection between blade wake and the downstream measurement points at $\psi \cong 30°$ (see [29] and [8] for a detailed analysis of this phenomenon). Predicted velocity trend are consistent among the different solvers. Nevertheless, *FUNAERO* predicts lower velocity magnitudes (9% and 8% at the inner and outer radius, respectively) with respect to ALM and CFD which are in closer agreement.

4. Conclusions

The aerodynamic behaviour of the state-of-the-art IEA 15 MW wind turbine rotor is herein investigated via specific implementations of four solvers based on BEMT (*AEOLIAN*), ALM (*OpenFOAM-v23*), free-wake Panel Method (*FUNAERO*) and blade-resolved CFD (*OpenFOAM-v23*) and by comparison with available BEMT and CFD data.

Good agreement of performance predictions is exhibited by the four solvers, with a variance among them of about 3%. Torque and thrust outcomes fall within a range of approximately 5.5% and 4% of the values provided by present BR-CFD, respectively. The observed deviations with respect to the available data are in line with the findings of the IEA Wind Task 47.

Predicted blade aeroloads are generally consistent and in reasonable agreement with the available reference data. The most significant deviations between high- and mid/low-fidelity solvers are observed primarily at the blade root. They arise due to the extensive flow separation on the blade suction side predicted by BR-CFD simulations. Additionally, BR-CFD and *FUNAERO* provide pressure distributions over the blades which exhibit perfect agreement

beyond a radius of 40 m.

A significant scattering of axial induction factor predictions is observed. The Azimuthal Averaging Technique and the Line Average Method used in BR-CFD results show how the latter is more effective in providing a physically consistent trend of the rotor wake induced velocity close to blade tip. It is also observed that panel-based computations using a small core radius (*i.e.*, the one used for the free-wake procedure) are consistent with the LAM model. Differently, an excessive increase of the vortex radius produces an excessive smoothing of the induction at the tip, yielding predictions more similar to AAT. These are critical aspects to be considered when higher-fidelity models are used to estimate the induction factors to be provided as input to BEMT- or ALM-based approaches.

Flow-field features past the rotor are more challenging to capture accurately. A good agreement by the geometry-resolved codes from upstream the rotor disk up to $x/R = 0.3$ downstream is exhibited, except where the effects of blade root separation (not modelled by the Panel Code) become significant. A more detailed study on the effect of extending the wake refinement zone for CFD simulations is advisable to enhance confidence in the prediction of wake resolution and induction in future work.

Acknowledgments

This work has been partially supported by the Horizon Europe Project MARINEWIND, Grant no. 101075572 and by PNRR, Spoke 6 "Multiscale Modelling and Engineering Application" in CN1-HPC "National Center on HPC, Big Data and Quantum Computing" programme. The authors wish to thank Dr. B. Stoevesandt for providing IWES BR-CFD data.

References

[1] Boorsma K *et al.* 2023 *Wind Energy Science* **8** 211–230
[2] Bergua R *et al.* 2023 *Wind Energy Science* **8** 465–485
[3] Leishman J 2006 Principles of helicopter aerodynamics
[4] Sørensen J N and Shen W Z 2002 *Journal of Fluids Engineering* **124** 393–399
[5] Boorsma K, Hartvelt M and Orsi L M 2016 *J. Phys. Conf. Ser.* **753** 022030
[6] Castorrini A, Tieghi L, Barnabei V, Gentile S, Bonfiglioli A, Corsini A and Rispoli F *IOP Conference Series*
[7] Boorsma K, Greco L and Bedon G 2018 *J. Phys. Conf. Ser.* **1037** 062013
[8] Greco L and Testa C 2021 *Renewable Energy* **164** 444–459
[9] Calabretta A, Molica Colella M, Greco L and Gennaretti M 2016 *Wind Energy* **19** 2301–2319
[10] Gaertner E *et al.* 2020 *NREL/TP-5000-75698*
[11] Menter F R 1994 *AIAA journal* **32** 1598–1605
[12] Greenshields C 2023 Openfoam v11 user guide
[13] Greco L, Testa C, Cirrincione M, Pucci M and Vitale G 2015 *ECCE2015 proceedings* pp 1027–1034
[14] Morino L 1993 *Appl. Mech. Rev.* **46** 445–466
[15] Greco L, Muscari R, Testa C and Di Mascio A 2014 *J. Hydrodyn., Ser. B* **26** 780–795
[16] Hoffman J D 2001 *Numerical methods for engineers and scientists* 2nd ed
[17] Bachant P, Goude A, daa mec and Wosnik M 2019 turbinesfoam/turbinesfoam: v0.1.1
[18] Castorrini A, Morici V, Girolamo F D, Tieghi L, Barnabei V F and Corsini A *IET Conference Proceedings*
[19] Bachant P, Goude A and Wosnik M 2018 (*Preprint* `1605.01449`)
[20] Martinez L *et al.* 2012 *50th AIAA Aerospace Sciences Meeting* p 900
[21] Aryan N, Greco L and Testa C 2023 *OSES23 Conference Proceedings*
[22] Ning S A 2014 *Wind Energy* **17** 1327–1345
[23] Hansen M O 2000 *Aerodynamics of wind turbines: rotors, loads and structure* vol 17 (Earthscan)
[24] Manwell J F, McGowan J G and Rogers A L 2010 *Wind energy explained: theory, design and application*
[25] Brent R P 1971 *The computer journal* **14** 422–425
[26] Buhl Jr M L 2005 Tech. rep. National Renewable Energy Lab. (NREL)
[27] Jost E, Klein L, Leipprand H, Lutz T and Krämer E 2018 *Wind Energy* **21** 807–822
[28] Hansen M *et al.* 1998 *Proceedings of the European wind energy conference* pp 499–502
[29] Micallef D, van Bussel G, Ferreira C S and Sant T 2013 *Wind Energy* **16** 529–544